SINUOSITY AS A MEASURE OF MIDDLE TROPOSPHERIC WAVINESS

by

Jonathan E. Martin[1], Stephen J. Vavrus[2], Fuyao Wang[2], and Jennifer A. Francis[3]

[1]Department of Atmospheric and Oceanic Sciences, University of Wisconsin-Madison
[2]Center for Climatic Research, University of Wisconsin-Madison
[3]Institute of Marine and Coastal Sciences, Rutgers University

Submitted to *Climate Dynamics*: January 1, 2015
Revised version submitted: June 8, 2015

ABSTRACT

Despite the importance of synoptic- to planetary-scale atmospheric waves in the production of organized mid-latitude weather systems, no widely accepted metric exists for quantifying the waviness of the large-scale circulation. The concept of sinuosity, borrowed from geomorphology, is introduced as a means of measuring the waviness of the mid-tropospheric flow using 500 hPa geopotential height contours. A simple method for calculating the sinuosity of the flow is presented and several broad characteristics of the flow are discussed.

First, the circulation is characterized by a maximum in waviness in the summer and a minimum in winter. Second, weakening (strengthening) of the wintertime mid-tropospheric zonal flow is shown to be associated with increased (decreased) waviness. Third, a strong negative correlation is found between the observed daily sinuosity and the daily Arctic Oscillation (AO) index in the cold season. Additionally, the DJF average sinuosity is shown to be highly correlated with the seasonal average AO index, suggesting that physical mechanisms that reduce (increase) the poleward height gradient, and correspondingly weaken (strengthen) the mid-latitude westerlies, may also encourage increased (reduced) waviness. The use of this metric to examine changes in the complexion of mid-latitude waviness in a changing climate is discussed.

1. Introduction

In recognition of the prominent role played by the mid-latitude westerlies in the general circulation of the Earth's atmosphere, Rossby and collaborators (1939) introduced the concept of the "zonal index"[1] as a measure of the strength of the zonal westerlies. Subsequent work by Namias (1950) examined what appeared to be a characteristic decline and recovery of the westerlies each winter in what he termed the "index cycle". This work represented the culmination of a series of investigations (e.g. Namias 1947a,b, Willett 1948, Wexler 1948) linking changes in the hemispheric circulation (evident in changes in the zonal index) to the equatorward movement of cold air during boreal winter. Central to this idea was the notion that strong, zonally oriented mid- to upper-tropospheric westerlies act to contain cold air at high latitudes so that cold-air outbreaks are afforded when the zonality of the flow relaxes.

The development of blocking ridges substantially interrupts the zonality of the flow and so has become a topic of considerable inquiry (e.g. Elliot and Smith 1949, Rex 1950ab, White and Clark 1975, Egger 1978, Austin 1980, Legenäs and Øakland 1983, Dole and Gordon 1983, Lupo and Smith 1995, Shabbar et al. 2001, Pelly and Hoskins 2003, Schwierz et al. 2004, Woollings et al. 2011, Masato et al. 2013, Barnes et al. 2014, Davini et al. 2014). Another feature at the center of studies of hemispheric circulation variability has been the circumpolar vortex (CPV) (e.g.

[1] Originally defined at sea-level as the average geostrophic wind in the latitude belt 35°N to 55°N. It is commonly evaluated aloft as well.

66 Markham 1985, Angell 1998, Davis and Benkovic 1992, Burnett 1993, Frauenfeld
67 and Davis 2003, Rohli et al. 2005, Wrona and Rohli 2007). As noted by Frauenfeld
68 and Davis (2003), assessment of variability in the size, strength and waviness of the
69 circulation can all be considered in terms of measurable characteristics of the CPV.

70 To our knowledge, only two studies of the variability of the CPV have directly
71 assessed the waviness of the mid-tropospheric flow. Rohli et al. (2005) borrowed a
72 measure from fluvial geomorphology – the circularity ratio (R_c) – to quantify the
73 waviness of the 5460m isohypse at 500 hPa (recommended by the study of
74 Frauenfeld and Davis 2003) for the month of January from 1959-2001. Wrona and
75 Rohli (2007) extended this analysis to DJF for each of those 43 cold seasons and
76 added analyses of the months of April, July, and October in order to uncover aspects
77 of the seasonality of the CPV, as depicted by this single 500 hPa isohypse.

78 High impact mid-latitude weather events and regimes are often associated
79 with large-amplitude planetary waves, as such patterns are dynamically linked to
80 robust cyclogenesis and anticyclogenesis events as well as the development of
81 blocked flows. In spite of this well-known relationship, no widely accepted metric
82 exists for quantifying the waviness of the circulation. Recent studies employing
83 gridded reanalysis data sets have offered reasonable suggestions. Francis and
84 Vavrus (2012) and Barnes (2013) incorporated measures of the maximum
85 meridional extent of 500 hPa isohypses (on both seasonal and daily time scales) as a
86 means of examining interannual trends in the complexion of middle tropospheric
87 waves. Screen and Simmonds (2013) employed a Fourier decomposition to first

88 characterize both the meridional and zonal amplitudes of waves in the mid-latitude
89 middle troposphere, and then examine temporal changes in these characteristics. In
90 the present paper we appropriate a measure common in geomorphology – *sinuosity*
91 – to measure the waviness of the mid-tropospheric flow using 500 hPa geopotential
92 height contours. As will be shown, calculation of this simple quantity ensures that
93 any departure from zonality in geostrophic streamlines, *not only the most extreme*
94 *departures*, is incorporated into a metric of hemispheric waviness. A seasonality in
95 the sinuosity of the flow is demonstrated, with a maximum in summer and
96 minimum in winter. Through consideration of a 500 hPa zonal index[2], a
97 characteristic weakening of the mid-tropospheric zonal wind in association with an
98 increase in sinuosity is demonstrated. Additionally, a strong negative correlation is
99 found between the observed daily sinuosity and the daily Arctic Oscillation (AO)
100 index in the cold season. Further, the winter (DJF) average sinuosity is shown to be
101 highly correlated with the seasonal average AO, suggesting that the physical
102 mechanisms that reduce (increase) the poleward height gradient and
103 correspondingly weaken (strengthen) the mid-latitude westerlies, may also foster
104 increased (reduced) waviness.

105 The purpose of this paper is to introduce a new tool for assessing changes in
106 the complexion of the large-scale circulation and to demonstrate fundamental
107 aspects of its utility. Accordingly, the paper is organized in the following manner.
108 In Section 2 we define sinuosity and describe both the method and data set used to

108

[2] The daily 500 hPa zonal index is calculated as the zonal average of the westerly geostrophic wind at 500 hPa in the latitude belt 35°-55°N.

calculate it. Aspects of the annual cycle in sinuosity, along with an emphasis on analysis of a time series of the previous 66 winter seasons, are presented in Section 3. The relationship between cold-season time series of sinuosity and the AO are also considered in that section. Finally, a summary and discussion of the results, including suggestions for future research, are offered in Section 4.

2. Data and Methodology

Morphological aspects of the meanders of rivers and streams is a subject in fluvial geomorphology. A simple measure of such meanders is known as sinuosity which is the ratio of the length of a segment of a stream to the length of the shortest distance between the endpoints of the segment (Leopold et al. 1964). A schematic example is given in Fig. 1. The extension of this idea employed in the present study depends upon calculation of the length of, and the area enclosed by, a given 500 hPa geopotential height contour (isohypse). Cutoff portions of any isohypse (i.e. cutoff lows or highs) are easily included in our measure of sinuosity because such features occupy a measurable area and their perimeters have finite lengths. We consider the waviness in a given mid-latitude flow to be a measure of the departure of its streamlines from zonality. Therefore, determination of the sinuosity of the flow along a geostrophic streamline (i.e. isohypse) begins by calculating the area enclosed by the given isohypse. Next, we compute an equivalent latitude for that isohypse. The equivalent latitude is that latitude poleward of which the area is

129 equal to the area enclosed by the given isohypse[3]. Finally, the sinuosity is defined as
130 the ratio of the length of the given 500 hPa isohypse to the circumference of its
131 equivalent latitude circle. An example is shown in Fig. 2. It follows from the
132 definition that the minimum value of sinuosity is 1.0 which describes a purely zonal
133 streamline (i.e. no waviness).

134 It has been suggested that shifting isohypses poleward in a warmer climate
135 might give rise to the illusion, when using sinuosity as a metric, of a change in
136 waviness when none is occurring. In order to evaluate this concern we conducted a
137 series of simple numerical experiments in which the sinuosity of hypothetical
138 isohypses, characterized by a varying number of deep and shallow square waves,
139 were carefully examined. The simplest case of a single modest square wave is
140 shown in Fig. 3. Keeping the aspect ratio of the square wave constant upon moving
141 the isohypse from 35° to 40°N results in an 8.9° latitudinal depth at 40°N compared
142 to the original 10° at 30°N. The poleward encroachment of this waveform results in
143 a 0.24% increase in sinuosity at the higher latitude. We suggest this is well small
144 enough to ensure that the utility of sinuosity as a metric of waviness is not
145 compromised. Additional support for allaying the aforementioned concern comes
146 from recent work by Bezeau et al. (2014) who demonstrated that the daily
147 climatological variability in Northern Hemisphere 500 hPa height anomalies is
147

[3] If A is the area enclosed by a given isohypse, then the equivalent latitude, ϕ_E, is given by $\phi_E = \arcsin[1 - \frac{A}{2\pi R_e^2}]$, where R_e is the radius of the Earth. Reference to an equivalent latitude is reminiscent of an aspect of the measure of eddy amplitude employed by Nakamura and Zhu (2010) and Nakamura and Solomon (2010, 2011) in their development of a diagnostic formulation for finite-amplitude wave activity.

148 significantly greater than the long term increase in heights resulting from Arctic
149 amplification.

150 Though many prior investigations of the variability of the mid-tropospheric
151 circulation have considered the area of the circumpolar vortex, only Rohli et al.
152 (2005) and Wrona and Rohli (2007) explicitly considered the waviness. They did so
153 using a measure called the circularity ratio (R_c) defined as the area enclosed within
154 a given isohypse divided by the area poleward of a zonal ring whose perimeter is
155 identically the length of the given isohypse. They applied this measure to a single
156 500 hPa isohypse (546 dm) for 42 cold seasons (DJF) using observed mean monthly
157 500 hPa geopotential height analyses on a 5° x 5° latitude/longitude grid from
158 NCAR's Monthly Northern Hemisphere Tropospheric Analysis.[4] Their choice of the
159 5460 m isohypse was motivated by the desire to consistently sample the size and
160 shape of the circumpolar vortex within the main belt of the westerlies. As described
161 below, our study builds on these pioneering efforts to quantify atmospheric
162 waviness by expanding the analysis in time and space and by applying a more
163 physically based morphometric parameter.

164 We employ the NCEP/NCAR reanalysis (NRA) data (Kalnay et al. 1996). Note
165 that while direct comparisons of reanalysis values to observations is problematic
166 owing to lack of independent measures, the upper-level circulation in the NRA has
167 been found to be very similar to that of the reanalysis by the European Centre for
168 Medium Range Weather Forecasts (Archer and Caldeira, 2008) and other reanalyses

168

[4] These data are available at http://dss/ucar/edu/datasets/ds085.1

by Davini (2013). These data are available 4 times daily on a global 2.5° x 2.5° grid and are derived from a frozen state-of-the-art global assimilation system in conjunction with a database that includes in-situ and remotely sensed data (when available) both at the surface and at levels through the troposphere and stratosphere. The present study calculates the sinuosity of a collection of individual 500 hPa isohypses in a domain covering 20°N to 90°N, using daily average 500 hPa heights constructed from the four times daily data, from 1 January 1948 to 28 February 2014. In addition to calculating the sinuosity of individual 500 hPa isohypses, we also calculate the aggregate sinuosity of a set of 5 isohypses (576, 564, 552, 540, and 528 dm) in which the maximum 500 hPa geostrophic wind resides throughout the year. The aggregate sinuosity at a given time is simply the ratio of the sum of the lengths of all 5 isohypses to the sum of the circumferences of the 5 equivalent latitude circles at that time[5].

A note regarding the differences between circularity ratio and sinuosity as separate measures of the waviness is warranted. Calculation of circularity ratio for a given isohypse requires determination of a latitude, ϕ_P, at which the length of a zonal streamline is equal to the length of the isohypse. Since the *areal extent*, not the length, of a given isohypse is directly related to a first order atmospheric variable (i.e. average temperature in the underlying troposphere via the

187

[5] One can choose any set of consecutive isohypses to produce an aggregate sinuosity. The choice made here is motivated by a desire to sample in the main belt of the westerlies. The aggregate sinuosity here is given by $S_5 = \frac{[L_{576} + L_{564} + L_{552} + L_{540} + L_{528}]}{[EL_{576} + EL_{564} + EL_{552} + EL_{540} + EL_{528}]}$ where L is the length of the indicated isohypse and EL is the length of its corresponding equivalent latitude circle.

188 hypsometric relationship), we submit that sinuosity is a more physically relevant
189 measure of the waviness. Furthermore, the present analysis, in contrast to those by
190 Rohli et al. (2005) and Wrona and Rohli (2007), considers an annual cycle in
191 waviness, relates the waviness metric to an important mode of large-scale
192 atmospheric variability (the Arctic Oscillation), and incorporates a range of
193 isohypses to more comprehensively characterize the complexion of middle
194 tropospheric waves across a broader extratropical domain. The mathematical
195 relationship between the two measures is presented in the Appendix.

196 **3. Results**

197 In order to examine the waviness of the 500 hPa flow in as comprehensive a
198 manner as possible, the following analysis is split into two broad categories. We
199 first consider the results of the 5 contour aggregate sinuosity calculations and then
200 move to evaluation of the characteristics of individual isohypses.

201 *a. Aggregate sinuosity*

202 The 500 hPa aggregate sinuosity analysis presented here considers the 576,
203 564, 552, 540, and 528 dm geopotential height contours and will be referred to as
204 S_5[6]. Each of these contours encloses a certain amount of area. Equal area is
205 contained poleward of an equivalent latitude (ϕ_{EQ}) and the length of the zonal ring at
206 ϕ_{EQ} represents the shortest possible perimeter that can enclose the given amount of
207 area. The contour length of a given isohypse is determined by summing its
207

[6] The correlation of the seasonal (DJF) average zonal index with seasonal average S_5 is -0.651.

208 segments in each 2.5° x 2.5° grid box calculated using the Spherical Law of Cosines
209 formula;

210 $$L = a\cos[\sin\phi_1 \sin\phi_2 + \cos\phi_1 \cos\phi_2 \cos(\lambda_2 - \lambda_1)]R_e$$

211 where (ϕ_1, λ_1) and (ϕ_2, λ_2) represent the latitude and longitude coordinates where
212 the given isohypse intersects the boundaries of a grid box and R_e is the radius of the
213 Earth.

214 The analysis presented here focuses on the winter (DJF) as it is during this
215 season that the mid-latitude flow is at its energetic peak. The 66-year time series of
216 DJF-average aggregate sinuosity is shown in Fig. 4. Over the course of this time
217 series, a slight, and statistically insignificant, upward trend in the aggregate
218 sinuosity is apparent.

219 The exceptionally high values of sinuosity in 2009-10 and 2010-11, suggest a
220 possible relationship with the Arctic Oscillation (AO), which reached its strongest
221 negative phase in winter 2009-10. Because mid-latitude circulation during the
222 positive (negative) phase of the AO tends to be anomalously zonal (wavy), sinuosity
223 should be able to capture this behavior quantitatively. Employing the daily Arctic
224 Oscillation (AO) time series from 1 December 1950 to present, the correlation
225 between the daily aggregate sinuosity of the 500 hPa flow and the AO index for each
226 DJF season since 1950-51 is shown in Fig. 5. Twenty-three of 64 years exhibit a
227 strong inverse relationship ($r \leq -0.6$) between the AO index and our measure of
228 sinuosity. In 43 of the 64 years $r \leq -0.4$, indicating a moderate relationship between
229 the two time series. Additional insight into this relationship arises from

consideration of the seasonal average AO index compared to the seasonal average sinuosity, as shown in Fig. 6. It is clear that enhanced waviness in the 500 hPa flow is associated with a negative AO as the two time series are correlated at r = -0.52 (significant above the 99% confidence level).

Another, less direct, inference regarding waviness of the middle latitude flow can be discerned from the zonal index. Figure 7 shows the time series of the correlation between the daily aggregate sinuosity (S_5) and the zonal index (ZI) for each DJF season since 1948-49. In 26 (45) of the 66 years the two time series are correlated at r ≤ -0.6 (-0.4) though, as with the AO correlation just described, in nearly 1/3 of seasons the relationship between the two is rather weak.

b. Annual cycle of sinuosity

The annual cycle of waviness is another aspect of the large-scale behavior of the mid-latitude atmosphere that can be interrogated using sinuosity. An annual cycle of the aggregate sinuosity was constructed by taking each calendar day's average sinuosity over the 66-year time series. The results of this analysis are shown in Fig. 8. Immediately apparent is the fact that the aggregate sinuosity reaches its maximum in summer and its minimum in winter. In fact, there is a broad peak in waviness that characterizes the warm season (April to October) with peak values of S_5 near 1.9 in early July and a fairly flat period of minimum values (~1.45) occurring in DJF. Also of note is the near symmetry of sinuosity on either side of the peak value. Finally, the annual cycle of 500 hPa zonal index is overlaid with the daily average S_5 in Fig. 8 indicating the nearly perfect inverse relationship between

252 aggregate sinuosity and 500 hPa zonal wind speeds (they are correlated at r = -
253 0.9506).

254 The annual cycle of sinuosity for the 5 individual isohypses that compose the
255 aggregate are shown, along with the aggregate, in Fig. 9. There is a clear
256 dichotomous structure exhibited amongst these 5 time series. The 576 dm isohypse
257 (red) exhibits the smallest annual cycle in waviness with evidence of two separate
258 peaks, the most prominent one near August 1 and a secondary peak near mid-
259 October. The 564 dm isohypse (orange) is characterized by the sharpest peak
260 (maximizing in early July) but the tails of its annual cycle are not symmetric. The
261 sinuosity is much lower (near 1.3) from January ~15 March whereas it persists well
262 above 1.3 from mid-October to the end of December. A broad warm-season peak
263 also characterizes the 552 dm isohypse (blue) though it reaches its peak value in
264 mid-June. The warm season increase in sinuosity of this streamline also
265 demonstrates a double peak with the secondary maximum centered around August
266 1.

267 It must be noted that the calculation of daily average sinuosity for
268 individual isohypses includes only those days on which a value exists. This method
269 ensures that whenever the contour does not exist on a given day, its absence does
270 not dilute the average value of sinuosity for the calendar day. This is an important
271 qualification when considering the dramatically different annual cycles exhibited by
272 the 540 (green) and 528 dm (magenta) isohypses (Fig. 9). The areal extent of both
273 of these values of geopotential height shrinks dramatically in the warm season. In

fact, for a number of calendar days in late July, more than half of all years had a lower troposphere warm enough to preclude the existence of the 528 dm isohypse. Though this is not the case for the 540 dm isohypse[7], it displays a similar annual cycle of sinuosity. Careful examination of its annual distribution shows that with the approach of summer, the 540 dm isohypse, characterized in winter and spring by a broad polar cap with occasional cutoff "satellites" at low latitude, is transformed into a collection of small, isolated cutoffs. The daily number of distinct 540 dm cutoffs peaks in late May/early June. With continued warming of the hemisphere, the number and areal extent of the 540 dm cutoffs is reduced through July almost to the point of extinction. The reduction in the number and size of 540 dm features, which drastically shrinks the total 540 dm perimeter, greatly reduces the sinuosity of that streamline in July.

c. Relation of the annual cycle in S_5 to morphological features of the NH circulation

Cut-off lows (COLs) are closed cyclonic circulations in the upper troposphere that have become detached from, and often subsequently migrate equatorward of, the main westerlies (Gimeno et al. 2007). Conversely, cutoff highs (COHs) are closed anticyclonic circulations that migrate poleward, often as a result of wave breaking, and can promote the development of blocked flows. As described previously, our calculation of sinuosity takes explicit account of the contributions from COLs as well as COHs. Such features invariably increase the sinuosity of a

294

[7] July 25 is the calendar day with the highest number (3) of missing 540 dm isohypses. In the entire 66-year time series, there are a total of only 28 such days for 540 dm whereas there are 1934 such days for 528 dm.

295 given geopotential height contour to a degree dependent on the areal extent and
296 latitude of the cutoff and so contribute to increases in S_5 as well.

297 The seasonal cycle of aggregate sinuosity is consistent with the higher
298 incidence of mid-tropospheric COLs that characterizes the Northern Hemisphere
299 warm season (Parker et al. 1989, Bell and Bosart 1989, Wernli and Sprenger 2007,
300 Nieto et al. 2008). In fact, Nieto et al. (2008) found that 41% of all COLs identified in
301 the NCEP Reanalysis data from 1948-2006 occurred in JJA while only 17% occurred
302 in DJF. Additionally they found that the frequency of autumn (SON) COLs slightly
303 exceeds that of spring (see their Fig. 14). This is consistent with the secondary peak
304 in S_5 that appears in September/October in the present analysis (see Fig. 6).

305 Parker et al. (1989) also considered the distribution of 500 hPa closed
306 anticyclones in their 36 year climatology. Such features are substantially less
307 frequent than COLs. Though anticyclones needn't be closed to have a substantial
308 impact on sinuosity (e.g. high amplitude, open ridges greatly increase S_5), they found
309 that these disturbances are most frequent over the subtropics with highest
310 incidence in the warm season.

311 In order to quantify the contribution of cutoff isohypses to the annual cycle of
312 S_5, COLs and COHs in each of the 5 threshold isohypses were objectively identified
313 over the entire time series. We then recalculated S_5, excluding the influence of the
314 cutoffs. Since COLs are separated from the broader polar cap of heights below a
315 given threshold (Fig. 10a), the areal extent of such features was excluded from the
316 recalculation of equivalent latitude and the contour length around them was

317 excluded from the recalculation of the total contour length[8]. Since a COH is always
318 poleward of the southernmost edge of the distribution of a given isohypse (Fig.
319 10b), its presence contributes nothing to the area enclosed by that isohypse.
320 Consequently, for COHs no adjustment to equivalent latitude was required - instead,
321 only the length around COHs was excluded in the recalculation of S_5. The annual
322 cycle of the recalculated S_5 is shown along with the actual annual cycle in Fig. 11.
323 The analysis demonstrates that the presence of cutoffs in the warm season produces
324 a substantial increase in sinuosity. In fact, using the wintertime minimum in
325 average S_5 (1.41) as a baseline, cutoffs contribute ~31% to waviness at the peak of
326 the warm season (~July 1).[9] This influence is consistent with the much higher
327 frequency of both species of cutoffs during the warm season. Additionally, routine
328 perusal of 500 hPa maps makes clear that cutoffs nearly always develop within
329 flows characterized by elevated values of pre-cutoff waviness. Thus, the evidence
330 presented in Fig. 11 suggests that the development of cutoffs enhances the waviness
331 of the already wavier flow that characterizes the warm season.

332 The coincidence of these various synoptic-climatological features suggests
333 the following explanation for the seasonal cycle in sinuosity. As the minimally wavy
334 wintertime circumpolar vortex shrinks with the coming spring, cutoff lobes of low
335 geopotential height are orphaned at low latitudes where increasingly intense

335

[8] In addition, any isolated, continuous piece of the area enclosed by a given isohypse that was less than 62% of the total area enclosed by that isohypse on a given day was considered a COL.
[9] This influence was calculated as (S_5 – S_5 w/out cutoffs)/(S_5 – 1.41) which, for peak values near July 1, was 0.15/0.49.

insolation quickly relaxes their associated tropospheric cold anomalies and corresponding negative 500 hPa height anomalies. The warm season maximum in COLs and COHs accounts for a substantial portion of the summertime maximum in S_5. The late summer/early autumn presence of tropical cyclones, and their inevitable recurvature to middle-latitudes, provides a seasonally unique mechanism for the growth of mid-latitude ridges in that season that accounts for the secondary autumnal peak in sinuosity previously noted. Finally, it is hypothesized that the decline of sinuosity in the autumn transition to winter is a function of the absorption of cutoffs that results from the expansion of the circumpolar vortex as the hemisphere cools.

4. Discussion and Conclusions

Despite the fact that a substantial fraction of high impact mid-latitude weather events and regimes are associated with large-amplitude planetary waves (Screen and Simmonds 2014), no widely accepted metric exists for quantifying the waviness of the circulation. In this paper we have introduced the concept of sinuosity as a new tool for measuring waviness and applied it to a set of 500 hPa geopotential height contours that contain the maximum wind throughout the year.

A seasonality in the sinuosity of the flow has been demonstrated, with a maximum in summer and minimum in winter. This finding is consistent with the metric of high-amplitude wave patterns introduced by Francis and Vavrus (2015), which exhibits a similar annual cycle to that of S_5. It has also been demonstrated that a weakening of the mid-tropospheric zonal wind is often associated with an

increase in sinuosity. Additionally, a strong negative correlation exists between the observed daily sinuosity and the daily Arctic Oscillation (AO) index in the cold season. Further, the winter (DJF) average sinuosity is shown to be highly correlated with the seasonal average AO and the zonal index (ZI), suggesting that the physical mechanisms that reduce (increase) the poleward height gradient and correspondingly weaken (strengthen) the mid-latitude westerlies, may also foster increased (reduced) waviness.

We have calculated sinuosity based on 500 hPa height contours in this study as a means of characterizing the waviness of the broad, middle tropospheric flow. An extension of the method outlined here, that would more specifically assess the waviness of the tropopause-level jet stream, would be to calculate the sinuosity of contours of constant potential vorticity (PV) (referred to as *isertels* by Morgan and Nielsen-Gammon 1998). Since the tropopause-level jet is coincident with strong gradients in PV and is found on the low PV edge of such a gradient, calculation of the sinuosity of, for instance, the 2 PVU isertel would render a clear picture of the waviness of the tropopause-level jet stream itself. Complicating matters is the fact that two distinct species of tropopause-level jets, the polar and subtropical jet, are present nearly all the time. Isolation of one from the other can be accomplished through consideration of the isertels in separate isentropic layers that contain the separate jets. We plan to pursue this issue in future work.

Recent studies by Francis and Vavrus (2012, 2015), Barnes (2013), and Screen and Simmonds (2013) have examined the question of whether Arctic

amplification has caused planetary-scale waves to become wavier and less progressive resulting in more frequent blocking and associated severe weather. The question remains an open one at present, at least partially due to the lack of an accepted measure of waviness. Continued refinement of the sinuosity metric introduced here promises to enlighten that debate as well as other questions regarding the complexion of the middle-tropospheric flow in a changing climate. To that end, we are currently exploring the nature of the response in sinuosity to a variety of climate change scenarios using output from the CMIP5 suite of models.

Appendix

Circularity ratio (R_C) is defined as $R_C = \frac{A}{EQA}$, where A is the area enclosed by a given isohypse, and EQA is the area of the circle with the same perimeter as the isohypse.

Sinuosity (S) is defined as $S = \frac{L}{EQL}$, where L is the length of the given isohypse, and EQL is the circumference of the circle that encloses the same area as the isohypse.

Expressions for both of the known quantities (A and L, which are calculated from data) in terms of other relevant variables can be formulated. For instance,

$$L = 2\pi R_e \cos\phi_p$$

where ϕ_p is the latitude at which the circumference of a circle around the pole equals the length of the given isohypse. Thus, the variable EQA is given by

$$EQA = 2\pi R_e^{\,2}[1 - \sin\phi_p]$$

and the actual area enclosed by the isohypse is given by

$$A = 2\pi R_e^{\,2}[1 - \sin\phi_e],$$

where ϕ_e is the equivalent latitude derived from the initial calculation of the area enclosed by the isohypse.

Consequently, circularity ratio can be rewritten as

$$C = \frac{A}{EQA} = \frac{2\pi R_e^{\,2}[1 - \sin\phi_e]}{2\pi R_e^{\,2}[1 - \sin\phi_p]} = \frac{[1 - \sin\phi_e]}{[1 - \sin\phi_p]}. \qquad \text{(A1)}$$

408 Sinuosity can also be rewritten in terms of these two different latitudes as

409 $$S = \frac{L}{EQL} = \frac{2\pi R_e \cos\phi_p}{2\pi R_e \cos\phi_e} = \frac{\cos\phi_p}{\cos\phi_e} \quad \text{(A2)}$$

410 since $EQL = 2\pi R_e \cos\phi_e$ by definition. Thus, the relationship between R_C and S is

411 $$S^2 R_C = \frac{1+\sin\phi_p}{1+\sin\phi_e}. \quad \text{(A3)}$$

412

412

413 **REFERENCES**

414

415 Angell, J. K., 1998: Contraction of the 300 mbar north circumpolar vortex during
416 1963-1997 and its movement into the Eastern Hemisphere. *J. Geophys. Res.*,
417 **103**, 25887-25893.

418 Austin, J. F., 1980: The blocking of middle latitude westerly winds by planetary
419 waves. *Quart. J. Roy. Meteor. Soc.*, **106**, 327-350.

420 Archer, C. L., and K. Caldeira, 2008: Historical trends in the jet streams. *Geophys. Res.*
421 *Lett.*, **35**, L08803, doi:10.1029/2008GL033614.

422 Barnes, E. A., E. Dunn-Sigouin, G. Masato, and T. Woollings, 2014: Exploring recent
423 trends in Northern Hemisphere blocking. *Geophys. Res. Lett.*, **41**,
424 doi:10.1002/2013GL058745.

425 Barnes, E. A., 2013: Revisiting the evidence linking Arctic amplification to extreme
426 weather in midlatitudes. *Geophys. Res. Lett.*, **40**, 1-6,
427 doi:10/1002/GRL.50880.

428 Bell, G. D., and L. F. Bosart, 1989: A 15-year climatology of Northern Hemisphere
429 500 mb closed cyclone and anticyclone centers. *Mon. Wea. Rev.*, **117**, 2141-
430 2163.

431 Bezeau, P., M. Sharp, and G. Gascon, 2014: Variability in summer anticyclonic
432 circulation over the Canadian Arctic Archipelago and west Greenland in the

late 20th/early 21st centuries and its effect on glacier mass balance. *Int. J. of Clim*., doi:10.1002/joc.4000.

Burnett, A. W., 1993: Size variations and long-wave circulation within the January Northern Hemisphere circumpolar vortex: 1946-89. *J. Climate*, **6**, 1914-1920.

Davini, P., C. Cagnazzo, and J. A. Anstey, 2014: A blocking view of the stratosphere-troposphere coupling. *J. Geophys. Res*., **119(19)**, 11100-11115.

Davini, T. D., 2013: Atmospheric blocking and mid-latitude climate variability. Ph. D. dissertation, *Programme in Science and Management of Climate Change*, University of Foscari, Italy.

Davis, R. E., and S. R. Benkovic, 1992: Climatological variations in the Northern Hemisphere circumpolar vortex in January. *Theoretical and Applied Climatology*, **46**, 63-73.

Dole, R. M., and N. D. Gordon, 1983: Persistent anomalies of the extratropical Northern Hemisphere wintertime circulation: Geographical distribution and regional persistence characteristics. *Mon. Wea. Rev*., **111**, 1567-1586.

Egger, J., 1978: Dynamics of blocking highs. *J. Atmos. Sci*., **35**, 1788-1801.

Elliot, R. D., and T. B. Smith, 1949: A study of the effect of large blocking highs on the general circulation in the northern hemisphere westerlies. *J. Meteor*., **6**, 67-85.

452 Francis, J. A., and S. J. Vavrus, 2012: Evidence linking Arctic amplification to extreme
453 weather in mid-latitudes. *Geophys. Res. Lett.*, **39(6)**, L06801,
454 doi:10/1029/2012GL051000.

455 _____, and _____, 2015: Evidence for a wavier jet stream in response to rapid arctic
456 warming. *Environ. Res. Lett.*, **10**, 014005, doi:10.1088/1748-
457 9326/10/1/014005.

458 Frauenfeld, O. W., and R. E. Davis, 2003: Northern Hemisphere circumpolar vortex
459 trends and climate change implications. *J. Geophys. Res.*, **108**, 4423-
460 doi:10.1029/2002/JD002958.

461 Gimeno, L., R. M. Triego, P. Ribera, and J. A. Garcia, 2007: Editorial: Special issue on
462 cut-off low systems (COL). *Meteorol. Atmos. Phys.*, **96**, 1-2,
463 doi:10.1007/s00703-006-0216-5.

464 Kalnay, E. et al., 1996: The NCEP/NCAR 40-year reanalysis project. *Bull. Amer.*
465 *Meteor. Soc.*, **77**, 437-471.

466 Lejenäs, H., and H. Øakland, 1983: Characteristics of northern hemisphere blocking
467 as determined from long time series of observational data. *Tellus*, **35A**, 350-
468 362.

469 Lupo, A. R., and P. J. Smith, 1995: Climatological features of blocking anticyclones in
470 the Northern Hemisphere. *Tellus*, **47A**, 439-456.

471 Markham, C. G., 1985: A quick and direct method for estimating mean monthly
472 global temperatures from 500 mb data. *Professional Geographer*, **37**, 72-74.

473 Martin, J. E., 2015: Contraction of the Northern Hemisphere, lower tropospheric,
474 wintertime cold pool over the last 66 years. *J. Climate*, **28**, (submitted).

475 Masato, G., B. J. Hoskins, and T. J. Woollings, 2013: Winter and summer Northern
476 Hemisphere blocking in CMIP5 models. *J. Climate*, **26**, 7044-7059.

477 Morgan, M. C., and J. W. Nielsen-Gammon, 1998: Using tropopause maps to diagnose
478 midlatitude weather systems. *Mon. Wea. Rev*., **126**, 2555-2579.

479 Nakamura, N. and D. Zhu, 2010: Finite-amplitude wave activity and diffusive flux of
480 potential vorticity in eddy-mean flow interaction. *J. Atmos. Sci*., **67**, 2701-
481 2716.

482 _____, and A. Solomon, 2010: Finite-amplitude wave activity and mean flow
483 adjustments in the atmospheric general circulation. Part I: Quasigeostrophic
484 theory and analysis. *J. Atmos. Sci*., **67**, 3967-3983.

485 _____, and _____, 2011: Finite-amplitude wave activity and mean flow adjustments in
486 the atmospheric general circulation. Part II: Analysis in the isentropic
487 coordinate. *J. Atmos. Sci*., **68**, 2783-2799.

488 Namias, J., 1950: The index cycle and its role in the general circulation. *J. Meteor*., **7**,
489 130-139.

490 Namias, J., 1947a: Physical nature of some fluctuations in the speed of the zonal
491 circulation. *J. Meteor*., **4**, 125-133.

492 Namias, J., 1947b: Characteristics of the general circulation over the northern
493 hemisphere during the abnormal winter of 1946-47. *Mon. Wea. Rev*., **75**, 145-
494 152.

495 Nieto, R., M. Sprenger, H. Wernli, R. M. Triego, and L. Gimeno, 2008: Identification
496 and climatology of cut-off lows near the tropopause. *Trends and Directions in*
497 *Climate Research:* Ann. N. Y. Acad. Sci. 1146: 256-290,
498 doi:101196/annals.1446.016.

499 Parker, S. S., J. T. Hawes, S. J. Colucci, and B. P. Hayden, 1989: Climatology of 500 mb
500 cyclones and anticyclones, 1950-85. *Mon. Wea. Rev*., **117**, 558-570.

501 Pelly, J., and B. J. Hoskins, 2003: A new perspective on blocking. *J. Atmos. Sci*., **60**,
502 743-755.

503 Rex, D. F., 1950a: Blocking action in the middle troposphere and its effect upon
504 regional climate. Part I: An aerological study of blocking action. *Tellus*, **2**, 196-
505 211.

506 Rex, D. F., 1950b: Blocking action in the middle troposphere and its effect upon
507 regional climate. Part II: The climatology of blocking action. *Tellus*, **2**, 275-
508 301.

509 Rohli, R. V., K. M. Wrona, and M. J. McHugh, 2005: January northern hemisphere
510 circumpolar vortex variability and its relationship with hemispheric
511 temperature and regional teleconnections. *Int. J. Climatol*., **25**, 1421-1436.

512 Rossby, C.-G., and collaborators, 1939: Relations between variations in the intensity
513 of the zonal circulation of the atmosphere and the displacements of the semi-
514 permanent centers of action. *J. Marine Res*., **2**, 38-54.

515 Schwierz, C., M. Croci-Maspoli, and H. C. Davies, 2004: Perspicacious indicators of
516 atmospheric blocking. *Geophys. Res. Lett*., **31**, L06125,
517 doi:10.1029/2003GL019341.

518 Screen, J. A., and I. Simmonds, 2013: Exploring links between Arctic amplification
519 and mid-latitude weather. *Geophys. Res. Lett*., **40**, 1-6,
520 doi:10.1002/GRL.50174.

521 _____, and _____, 2014: Amplified mid-latitude planetary waves favour particular
522 regional weather extremes. *Nat. Clim. Change*, **4**, 704-709.

523 Shabbar, A., J. Huang, and K. Higuchi, 2001: The relationship between the wintertime
524 North Atlantic Oscillation and blocking episodes in the North Atlantic. *Int. J.*
525 *Climatol*., **21**, 355-369.

526 Wernli, H., and M. Sprenger, 2007: Identification and ERA-15 climatology of
527 potential vorticity streamers and cutoffs near the extratropical tropopause*. J.*
528 *Atmos. Sci.*, **64**, 1569-1586.

529 Wexler, H., 1948: A note on the record low temperature in the Yukon Territory
530 January-February 1947. *Bull. Amer. Meteor. Soc*., **29**, 547-550.

531 White, W. B., and N. E. Clark, 1975: On the development of blocking ridge activity
532 over the central North Pacific. *J. Atmos. Sci*., **32**, 489-502.

533 Willett, H. C., 1948: Pattersn of world weather changes. *Trans. Amer. Geophys. Union*,
534 **29**, 803-809.

535 Woollings, T., J. G. Pinto, and J. A. Santos, 2011: Dynamical evolution of north Atlantic
536 ridges and poleward jet stream displacements. *J. Atmos. Sci*., **68**, 954-963.

537 Wrona, K. M., and R. V. Rohli, 2007: Seasonality of the northern hemisphere
538 circumpolar vortex. *Int. J. Climatol*., **27**, 697-713.

539

539 FIGURE CAPTIONS

540 Fig. 1 Schematic illustrating the concept of sinuosity. $\boldsymbol{S_{AB}}$ is the ratio of the length of
541 the blue contour to the length of the red line segment AB.

542 Fig. 2 Blue line is the daily average 552 dm geopotential height contour at 500 hPa
543 on 18 January 2014. The area enclosed by that line is equal to the area enclosed by
544 the red circle (the equivalent latitude). $\boldsymbol{S_{552}}$ is equal to the ratio of the length of the
545 blue line to the length of the red line (1.2719).

546 Fig. 3 Schematic illustration of the negligible effect that poleward migration of
547 isohypses has on sinuosity of a given contour. Original contour (in red) is zonal at
548 35N with a square wave of latitudinal depth 10. Displace contour (in blue) is zonal
549 at 40N with square wave whose aspect ratio (longitudinal extent/latitudinal extent)
550 is identical to original wave. The displaced contour has sinuosity 1.0024 times that
551 of original contour.

552 Fig. 4 Time series of DJF season averaged, aggregate sinuosity from 1948-49 to
553 2013-14.

554 Fig. 5 Time series of correlation coefficient, r, between the daily AO index and the
555 daily value of 500 hPa sinuosity (S_5) from 1950-51 to 2013-14. Green (blue) dots
556 represent seasons with r < -0.4 (-0.6).

557 Fig. 6 Time series of DJF seasonal averaged AO index (red) compared to DJF
558 seasonal averaged sinuosity (S_5) (blue). The two time series are correlated with r =
559 -0.520, significant above the 99% level.

560 Fig. 7 Time series of correlation coefficient, r, between daily zonal index (ZI) and the
561 daily value of 500 hPa aggregate sinuosity (S5) from 1948-49 to 2013-14. Green (blue)
562 dots represent seasons with $r < -0.4$ (-0.6).

563 Fig. 8 Daily average aggregate sinuosity (solid black line) derived from 66-year
564 NCEP Reanalysis time series. Gray shaded region represents +/- 1σ around the
565 daily mean. Daily average 500 hPa zonal index (ZI in m s^{-1}, blue solid line) derived
566 from the same data set.

567 Fig. 9 Solid black line is the daily average aggregate sinuosity derived from 66-year
568 NCEP Reanalysis time series. Daily average sinuosity of individual geopotential
569 height contours in the set of 5 used in the aggregate calculation are indicated by the
570 labeled colored lines.

571 Fig. 10 Schematic of an isohypse characterized by (a) a cutoff low (COL) and (b) a cutoff
572 high (COH). The total area enclosed by the given isohypse in both panels is shaded blue.
573 For the COL in (a), that area is the sum of A and B while the total contour length is the
574 sum of the perimeters of A and B. Recalculation of S5 in this case requires subtraction of
575 area B from the total area and subtraction of perimeter B from the total contour length.
576 For the COH in (b), the total area is smaller. Recalculation of S5 in this case requires
577 only that the perimeter of C be subtracted from the total contour length.

578 Fig. 11 Solid black line is the daily average aggregate sinuosity derived from 66-year
579 NCEP Reanalysis time series. Gray line represents the daily average sinuosity calculated
580 upon excluding the contribution of cutoff lows and highs in the threshold isohypses. See

581 text for explanation.

582

583

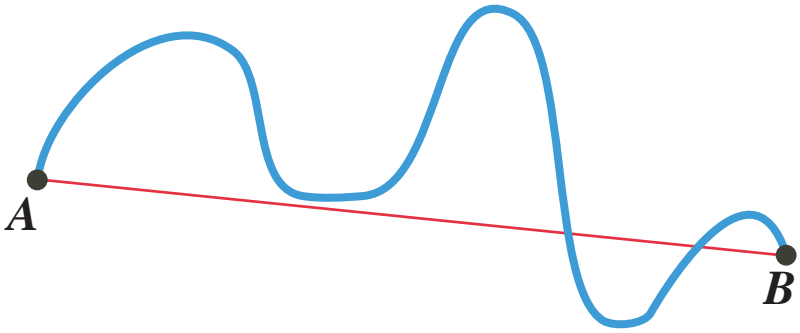

$$S_{AB} = \frac{\text{(Length of CONTOUR)}}{\text{(Length of SEGMENT)}}$$

Fig. 1 Schematic illustrating the concept of sinuosity. S_{AB} is the ratio
583 of the length of the blue contour to the length of the red line segment AB.

584

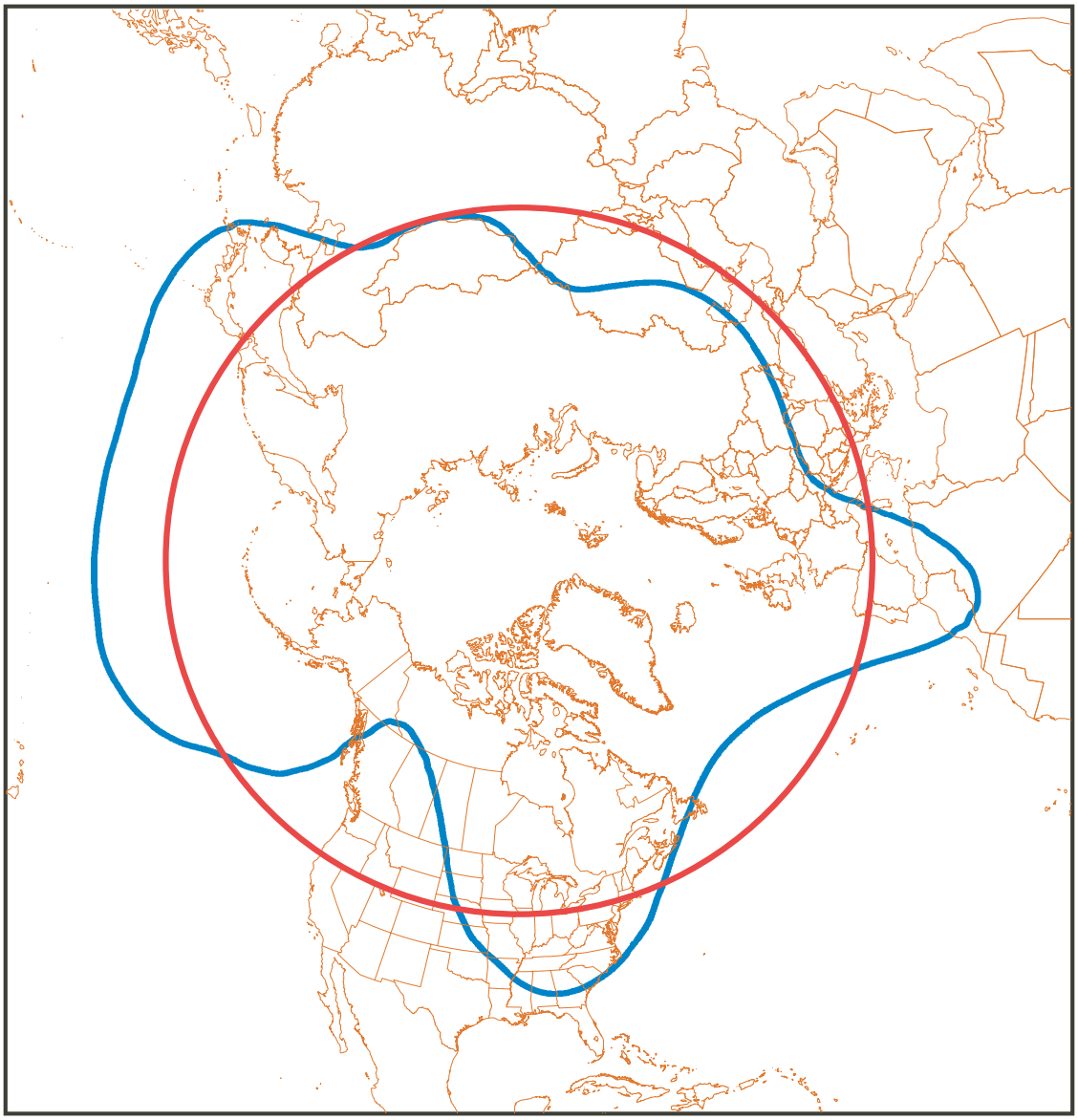

Fig. 2 Blue line is the daily average 552 dm geopotential height contour at 500 hPa on 18 January 2014. The area enclosed by that line is equal to the area enclosed by the red circle (the equivalent latitude). S_{552} is equal to the ratio of the length of the blue line to the length of the red line (1.2719).

584

585

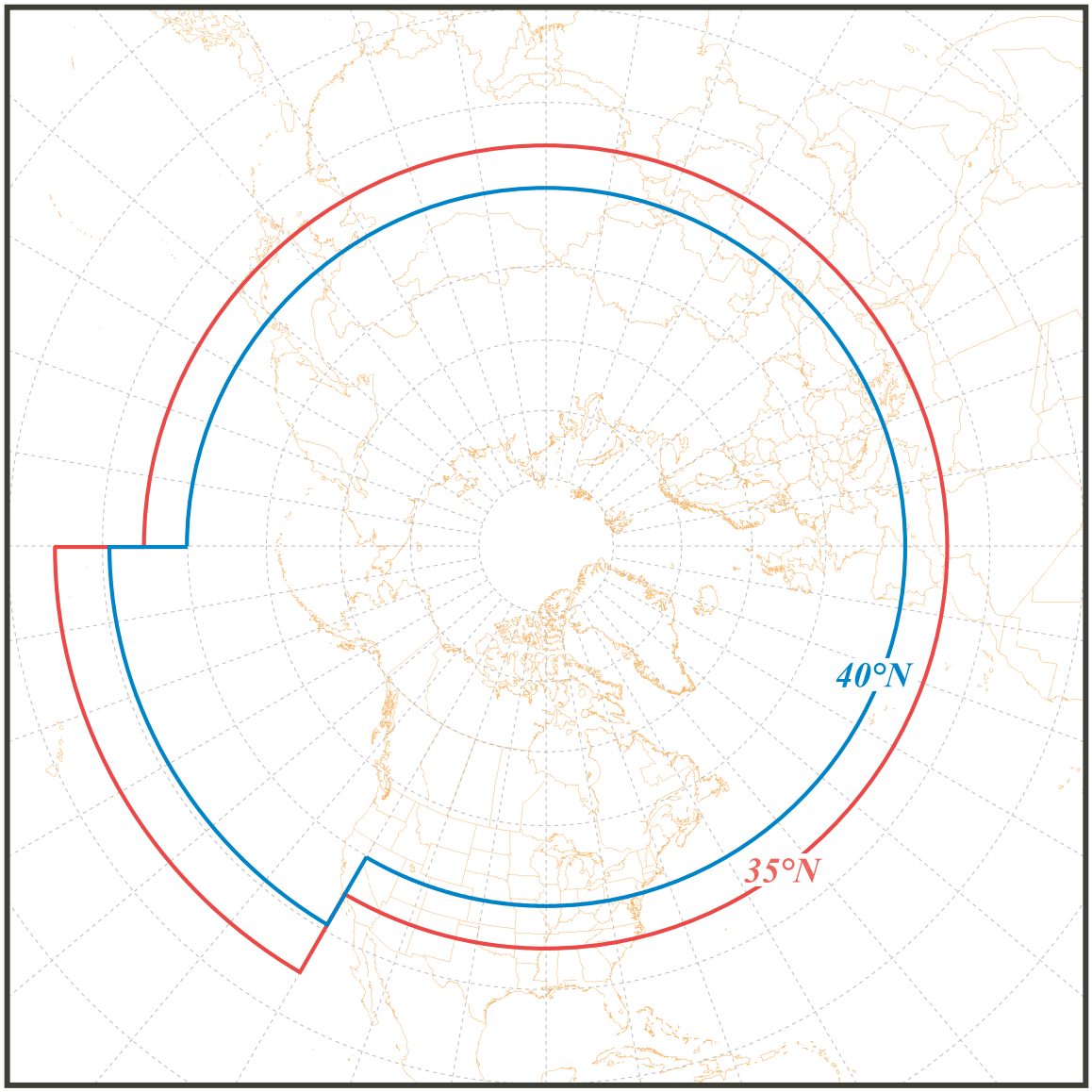

Fig. 3 Schematic illustration of the negligible effect that poleward migration of isohypses has on sinuosity of a given contour. Original contour (in red) is zonal at 35°N with a square wave of latitudinal depth 10°. Displaced contour (in blue) is zonal at 40°N with square wave whose aspect ratio (longitudinal extent/latitudinal extent) is identical to original wave. The displaced contour has sinuosity 1.0024 times that of original contour.

585

586

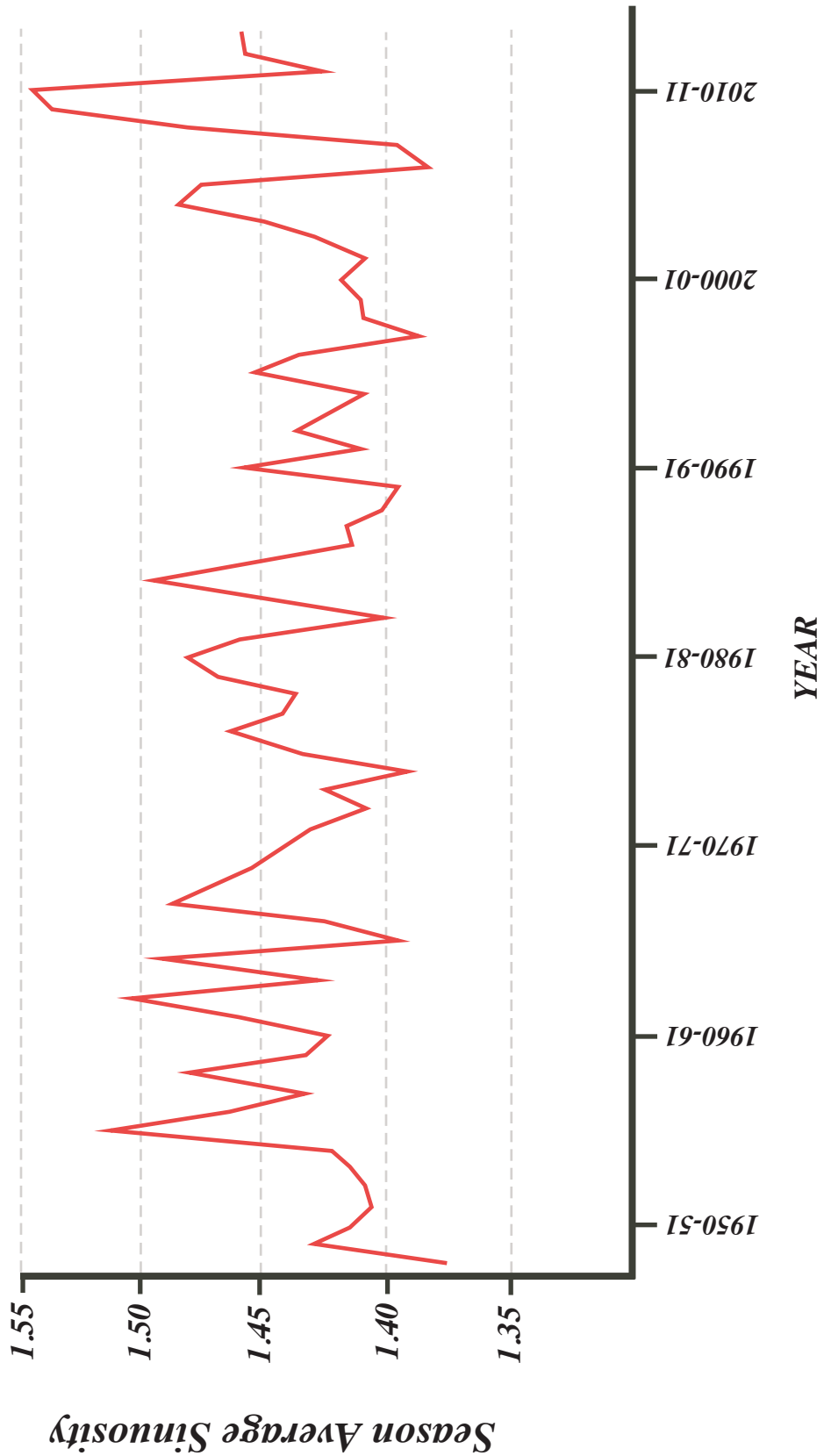

Fig. 4 Time series of DJF season averaged, aggregate sinuosity from 1948-49 to 2013-14.

586

587

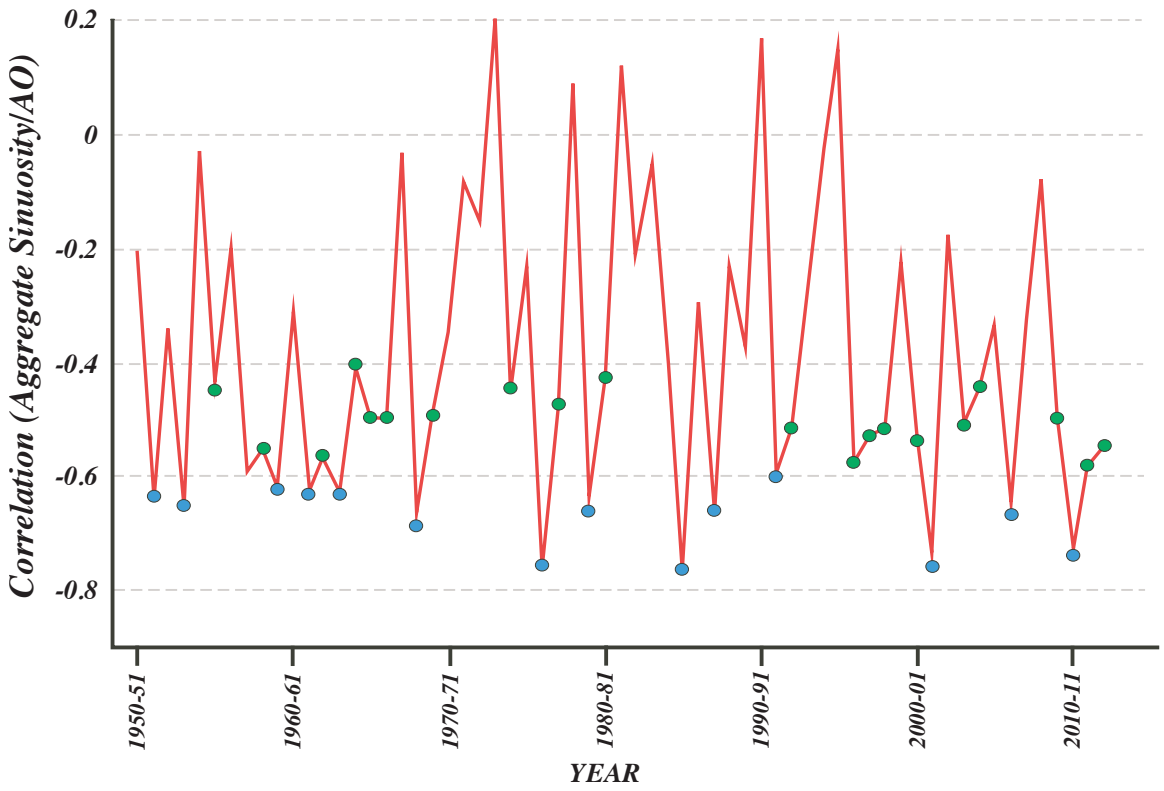

Fig. 5 Time series of correlation coefficient, r, between the daily AO index and the daily value of 500 hPa sinuosity from 1950-51 to 2013-14. Green (blue) dots represent seasons with r < -0.4 (-0.6).

587

588

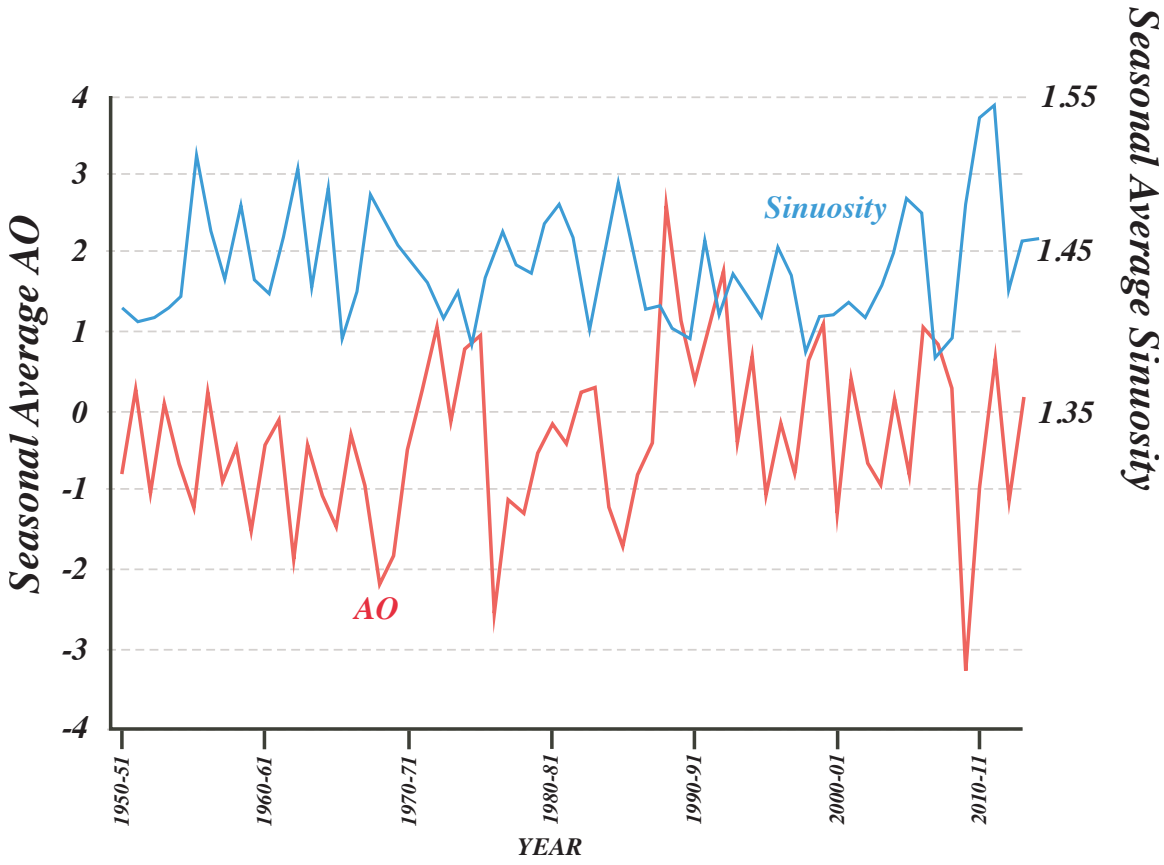

Fig. 6 Time series of DJF seasonal averaged AO index (red) compared to the DJF seasonal averaged sinuosity (blue). The two time series are correlated with r = -0.520, significant above the 99% level.

588

589

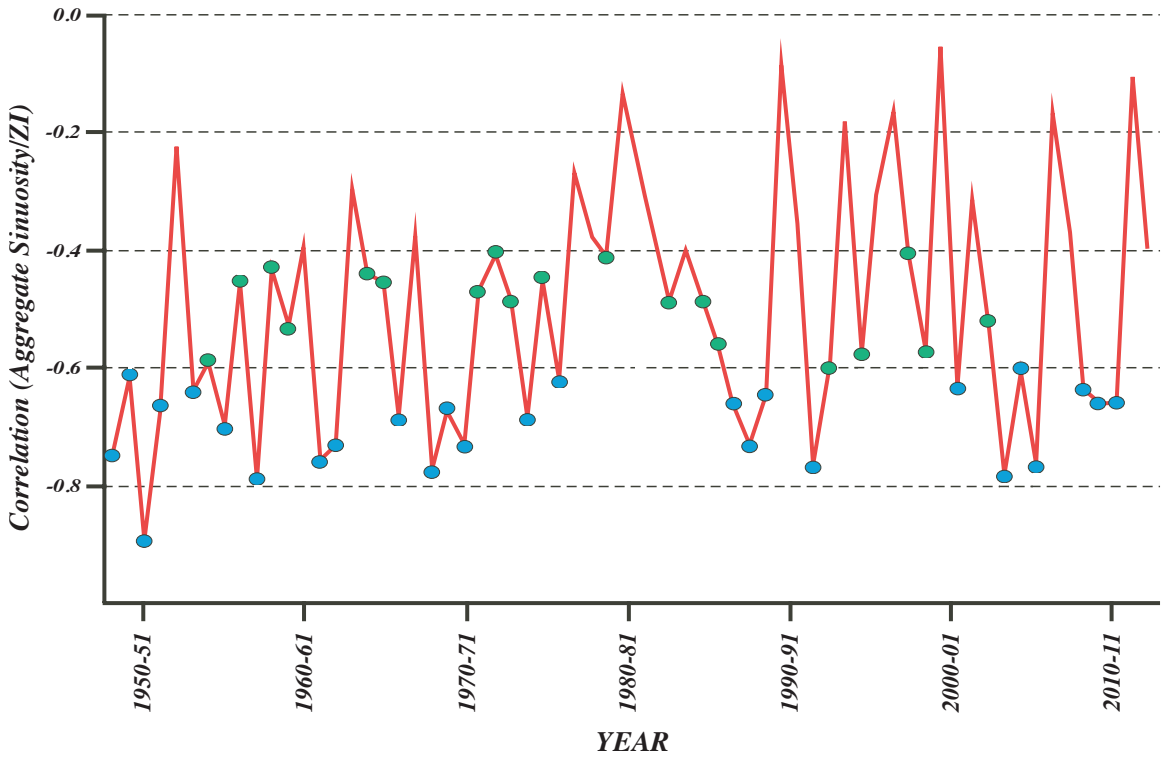

Fig. 7 Time series of correlation coefficient,r, between daily zonal index (ZI) and the daily value of 500 hPa aggregate sinuosity (S5) from 1948-49 to 2013-14. Green (blue) dots represent seasons with r < -0.4 (-0.6).

589

590

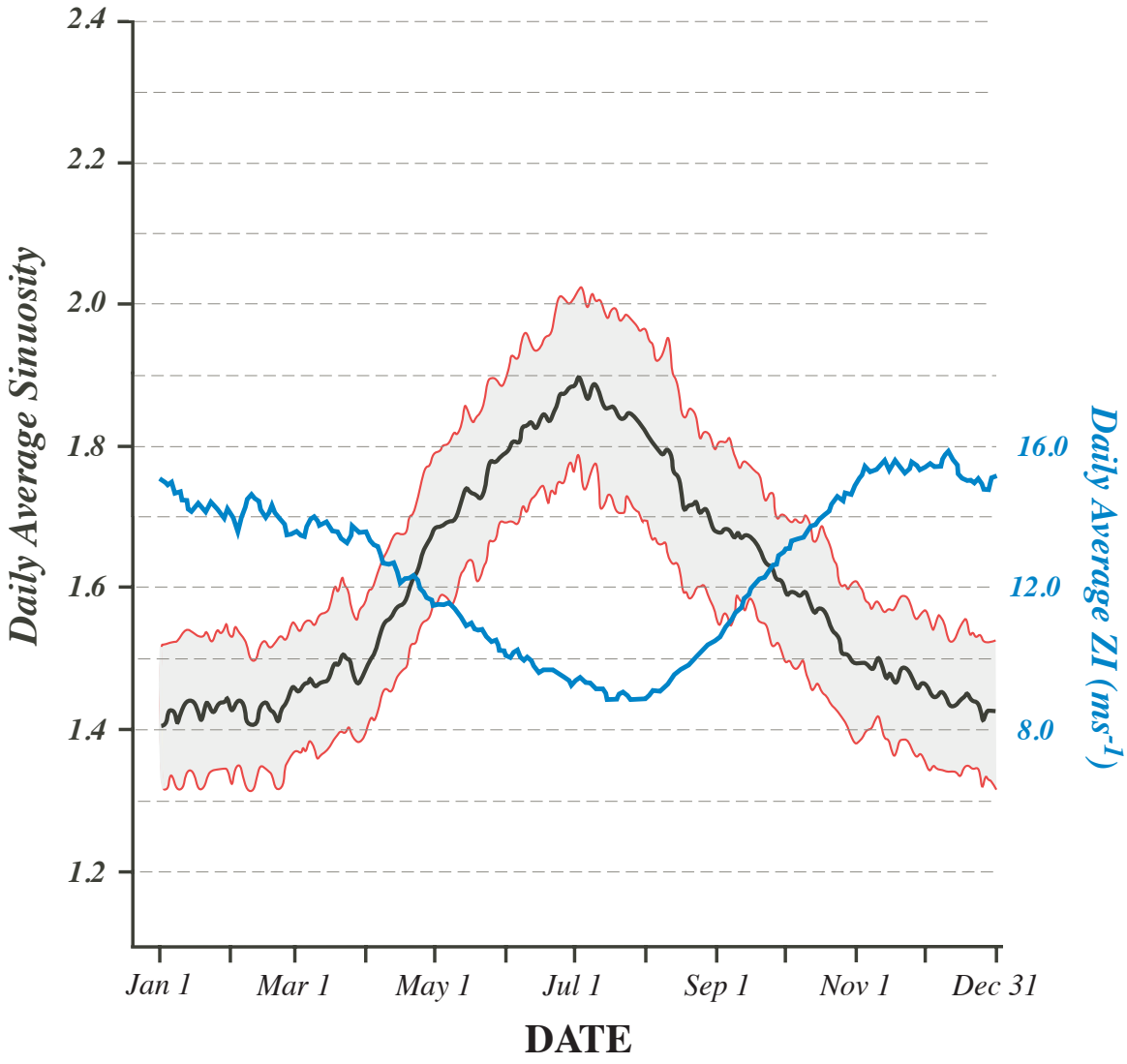

Fig. 8 Daily average aggregate sinuosity (solid black line) derived from 66-year NCEP Reanalysis time series. Gray shaded region represents +/- 1σ around the daily mean. Daily average 500 hPa zonal index (ZI in ms^{-1}, blue solid line) derived from the same data set.

590

591

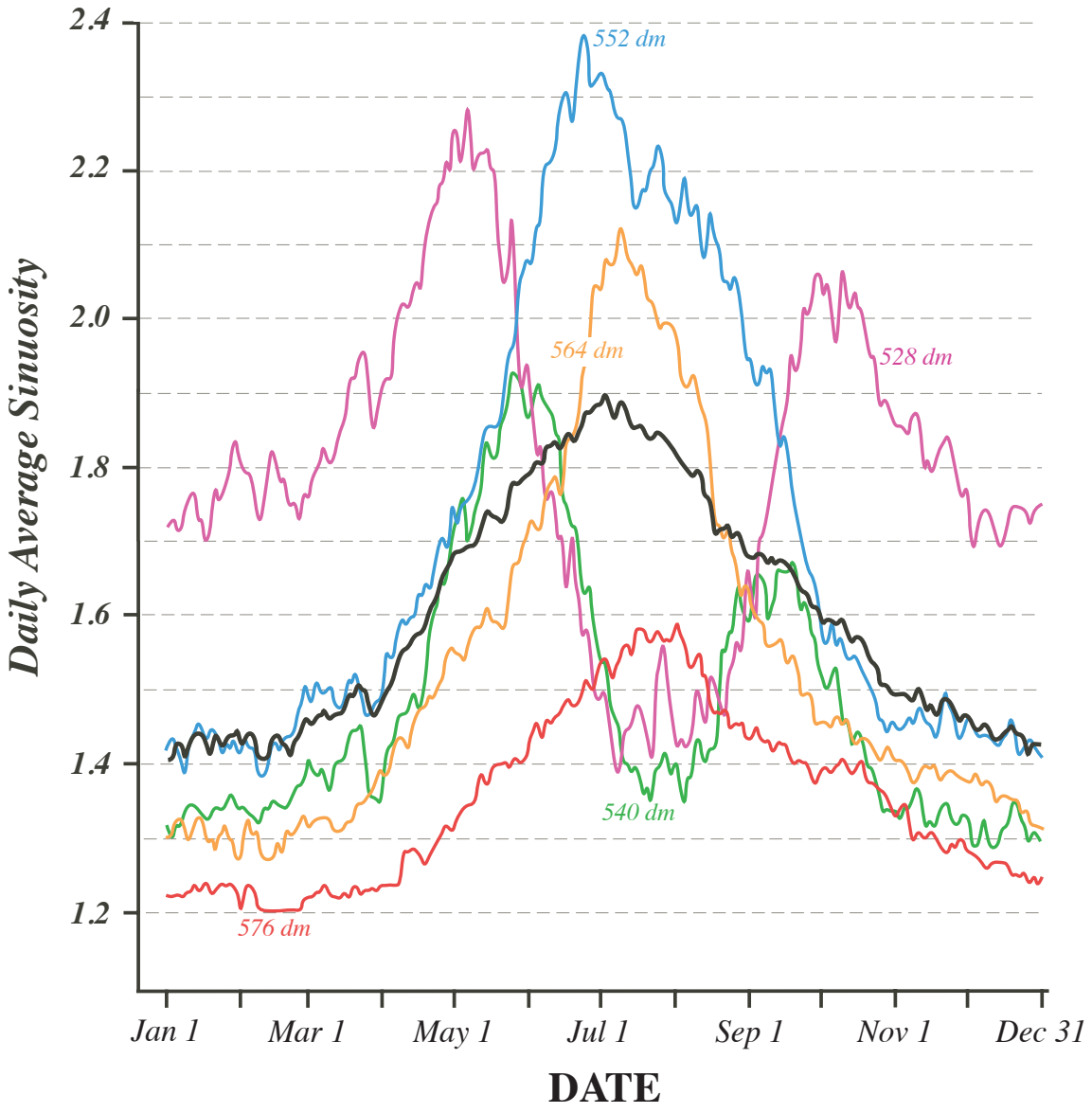

Fig. 9 Solid black line is the daily average aggregate sinuosity derived from 66-year NCEP Reanalysis time series. Daily average sinuosity of individual geopotential height contours in the set of 5 used in the aggregate calculation are indicated by the labeled colored lines.

591

592

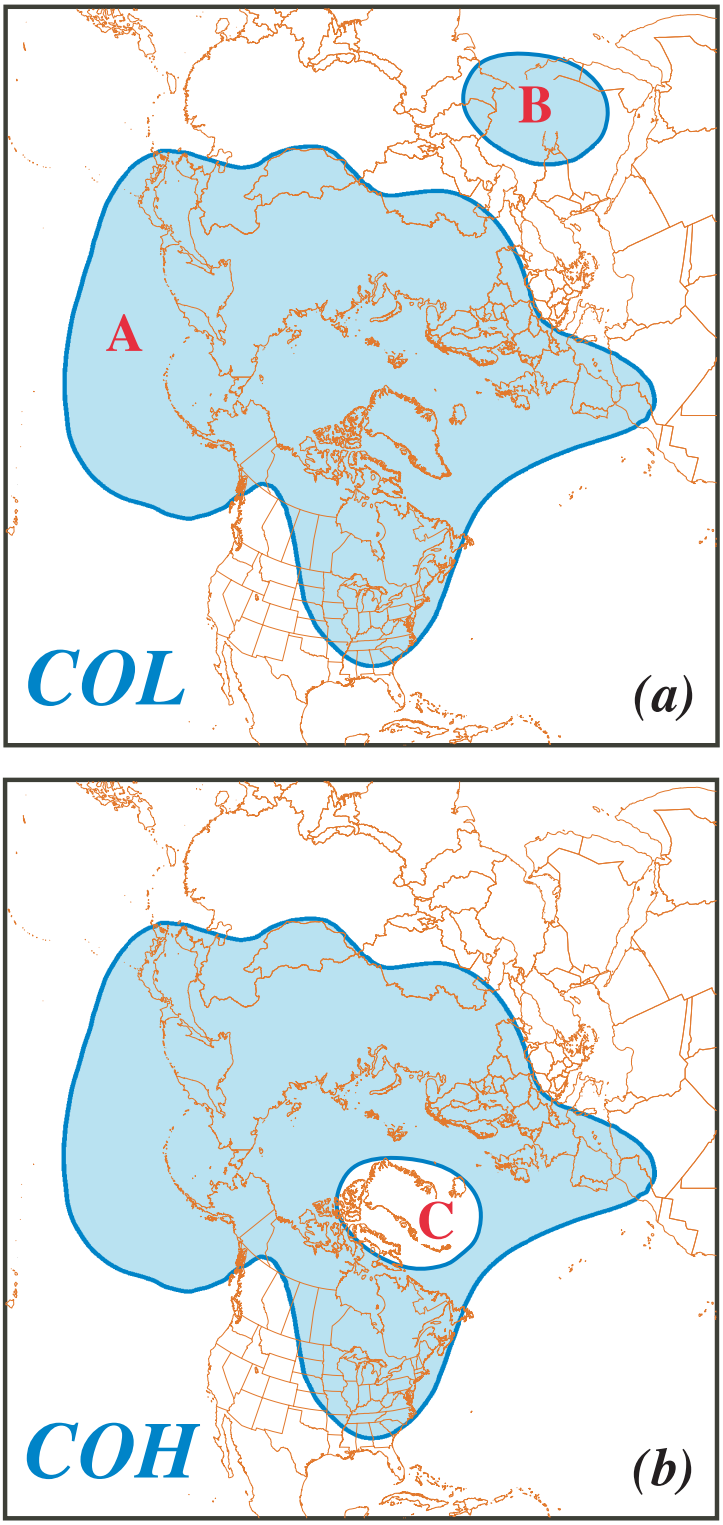

Fig. 10 Schematic of an isohypse characterized by (a) a cutoff low (COL) and (b) a cutoff high (COH). The total area enclosed by the given isohypse in both panels is shaded blue. For the COL in (a), that area is the sum of A and B while the total contour length is the sum of the perimeters of A and B. Recalculation of S_5 in this case requires subtraction of area B from the total area and subtraction of perimeter B from the total contour length. For the COH in (b), the total area is smaller. Recalculation of S_5 in this case requires only that the perimeter of C be subtracted from the total contour length.

592

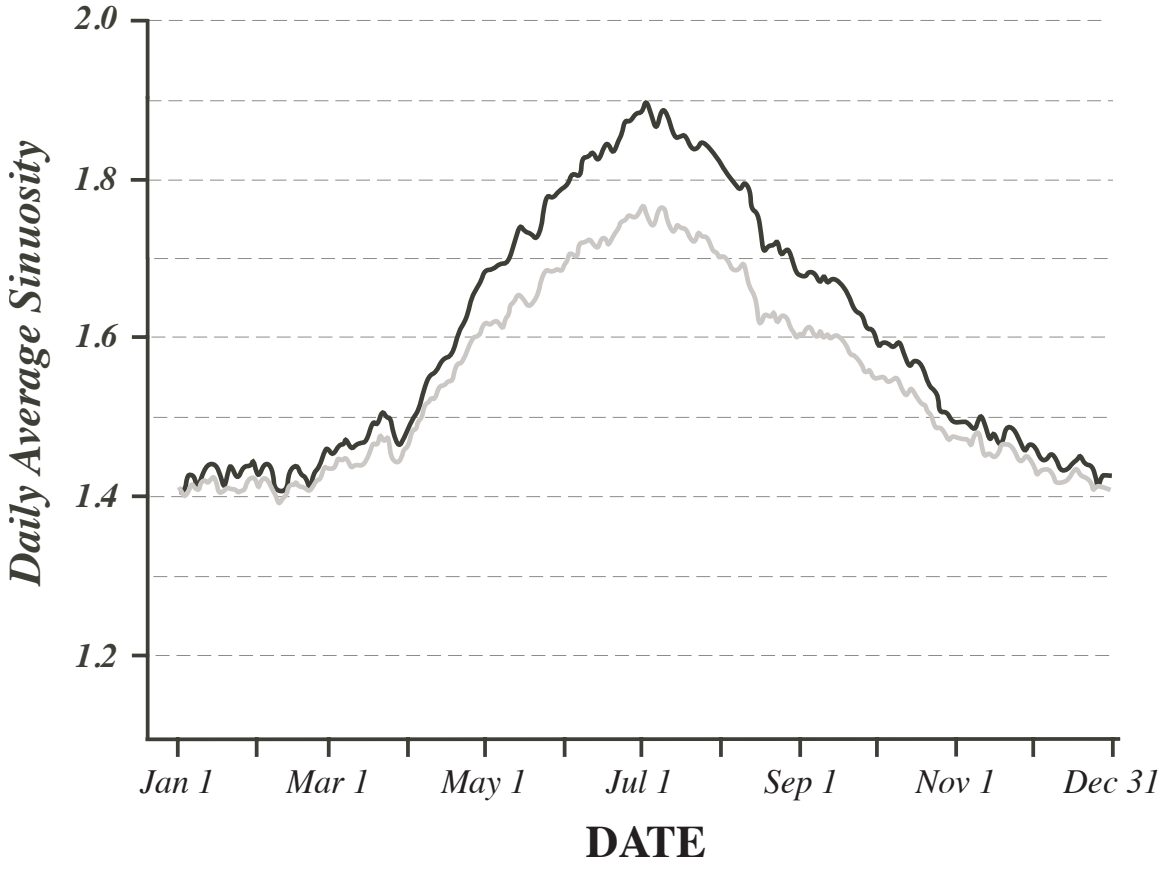

Fig. 11 Solid black line is the daily average aggregate sinuosity derived from 66-year NCEP Reanalysis time series. Gray line represents the daily average sinuosity calculated upon excluding the contribution of cutoff lows and highs in the threshold isohypses. See text for explanation.

593